ISAAC
Paper publication – Structural team
An active mass damper for seismic protection of structures

Full-scale shake table tests of a reinforced concrete building equipped with a novel servo-hydraulic active mass damper

Giovanni Rebecchi, Paolo M. Calvi, Alberto Bussini, Filippo Dacarro, Davide Bolognini, Luca Grottoli, Matteo Rosti, Francesco Ripamonti, Stefano Cii.

Abstract

This paper presents the results of an experimental program involving shake table testing of two full-scale reinforced concrete frame buildings. These tests were conducted to investigate the effectiveness and reliability of a newly proposed servo-hydraulic Active Mass Damper (AMD) that can be designed to enhance the target seismic performance of a building at multiple earthquake intensity levels.

The two nominally identical case-study buildings were intentionally designed to exhibit a "soft story" mechanism at the first level when subject to ground shaking of sufficient intensity, but one was equipped with the newly proposed AMD, installed on the roof. The two specimens were then subject to the same loading protocol consisting of a ground shaking sequence of varying intensity, with the seismic input consisting of a selected natural ground motion.

The experimental results demonstrated that the proposed AMD is extremely effective at enhancing building seismic performance. Specifically, the AMD provided peak displacement reductions in the order of 70% and was shown capable of absorbing more than 60% of the total input energy. As a consequence, the un-retrofitted structure suffered nontrivial structural and non-structural damage, while the AMD-retrofitted building remained virtually undamaged at all shaking intensities considered.

1 Introduction

Earthquakes are among the most destructive natural disasters that can cause major social and economic disruption to any given community. According to FEMA P-366 (2017) [1], earthquakes in the last decade alone have caused tens of thousands of casualties and hundreds of billions of dollars of economic impact worldwide.

Data collected following recent earthquakes show trends that indicate progressively increasing damage and losses due (among other factors) to the vulnerability of the older building stock, such as poorly engineered non-ductile concrete buildings.

A multitude of strategies have been proposed over the years that can be adopted to strengthen structurally deficient buildings enhancing their seismic performance. The selection of the optimal strengthening technique and the level of intervention is a rather complex procedure that is carried out on a case-by-case basis, considering the nature of the structural deficiencies to be addressed and other relevant factors.

In this context, "response-control" strategies based on the use of devices that can reduce the seismic demand by altering the dynamic properties of the structure and/or by absorbing part of the earthquake energy, have gained popularity over the past few decades. A variety of structural control systems have been proposed and are currently available in the literature, each presenting benefits and drawbacks. They are normally grouped in three broad categories, namely passive, semi-active and active devices, based on the fundamental principles governing their behavior and on their overall characteristics.

Examples of passive vibration control devices ([2]) include base isolators ([3], [4]), viscous, hysteretic and friction dampers ([5] and [6]), and tuned mass dampers ([7]). Passive devices enhance the seismic performance of a structure primarily by absorbing part of the input energy of the earthquake, thus reducing the seismic demand on the structural elements. The dissipation of energy occurs through a variety of mechanisms that depend on the nature of the damper utilized. Common energy dissipation mechanisms include yielding of mild steel, viscoelastic action in rubber-like materials, shearing of viscous fluid, sliding friction, etc. In addition to dissipating part of the input seismic energy, base isolators modify the period of vibration of the structure shifting its response such that the seismic demand on the system is reduced.

Evidently, passive control devices have no feedback capability between them, structural elements, and the input. Nevertheless, passive control systems are generally seen as effective at mitigating the effects of earthquakes and have been deployed relatively broadly. The main drawback they are typically attributed is their invasiveness, as their installation in existing structures may present a series of practical difficulties.

Semi-active control systems possess some of the features of passive devices, but their response can be "actively" adjusted according to the feedback from sensors that measure the excitation and/or the response of the structure. They typically rely on a small external power source but can continue to function in passive mode in the event of power failure.

Available semi-active devices are hydraulic dampers, controllable friction dampers, controllable fluid dampers and semi-active tuned mass dampers, among others.

Examples of studies that can be found in the literature pertaining to semi-active devices include [8], [9] and [10]. Reference [8] presents a position-controlled semi-active friction damper for seismic structures whereby the slip force is altered in real time, according to structural response of the system. References [9] and [10] discuss semi-Active Tuned Mass Dampers based on smart materials (e.g., magnetorheological fluids) that can change their mechanical properties such as damping or stiffness, as soon as a certain magnetic field is applied. Many other examples are available in the

ISAAC
Paper publication – Structural team
An active mass damper for seismic protection of structures

scientific literature that are omitted here for the sake of brevity. Interested readers can refer to [11], [12], [13], [14], [15], [16], [17], [18], [19], [20] and [21], among others.

Semi-active control systems have gained popularity in recent years because of their versatility and because they can achieve control effect similar to active systems (discussed below), while improving upon the performance of their passive counterparts. Their main limitation is represented by their reduced working range and by their efficiency, which is generally lower than that of fully active devices.

Active control systems provide protection of a building by generating forces that counterbalance the forces induced by an earthquake. These forces are generated by electro-mechanical or electro-hydraulic actuators based on the feedback response from the structure, and they require a higher power source compared to the semi-active devices. Active vibration control systems are gaining increasing traction because of their flexibility and versatility ([22], [23], [24] and [25]). For instance, active control systems can be simultaneously designed for different performance objectives and can be employed in a wide range of operations depending on the actuator working range ([26] and [27]).

Examples of active control systems for civil engineering applications include active brace systems, active tendon systems, active isolation systems and active mass dampers. Active mass dampers (see Fig. 1), also referred to as Active Mass Drivers (AMDs) are most relevant for the study presented in this paper and are thus briefly discussed herein. An AMD consists of an inertial mass driven by a linear servo-actuator or by a counter-rotating mass [28].

Similar to passive TMDs, AMD devices are usually installed on the roof of the building and enhance the building performance by absorbing part of the earthquake input energy by generating a counteracting control force based on the chosen control law. In some cases, several AMDs are used simultaneously, resulting in a Multiple-Input Multiple-Output (MIMO) system [29].

One of the earliest notable AMD studies was conducted by Dyke et al. ([30]), who investigated via shake table test the use of an AMD on a three-story frame scale model. The AMD employed in [30] consisted of a small hydraulic actuator, with inertial masses connected to the end of the actuator rod. Similar AMD mechanisms have been employed in other research programs (e.g., [31] and [32] among others).

AMD solutions that rely on electric servo actuation systems have also been proposed and implemented [33]. The electric actuators in AMDs can either make use of linear electrical motors or rotational motors. Both types have been employed in full-scale structures for more than a decade ([34] and [35]). Applications specific to AMDs driven by a linear servomotor can be found in [36] and [37], while examples of application of a rotational electric motor are available in [38] and [39]. Reference [39] in particular, discusses the case study of an AMD with a 38 ton steel mass installed atop a 114 m tall building in Tokyo, Japan (*Figure 1*).
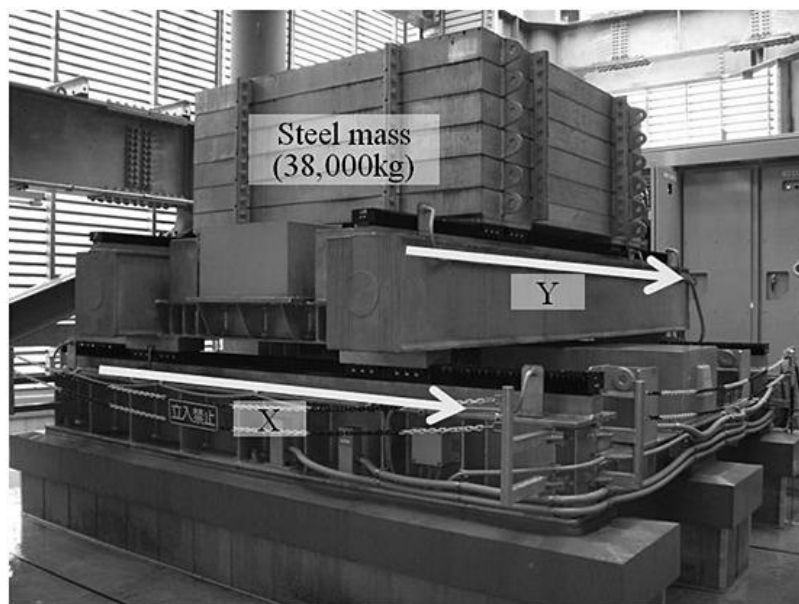
Figure 1 – Application Example of an Active Mass Damper [39]

All experimental and numerical evidence collected over time shows that buildings equipped with AMDs can achieve high performance, and that AMDs made with electric actuators have benefit that include easier maintenance, less space needed for installation and lower cost. Their main limitation is that they can only generate lower forces ([39], [40]). Consequently, electric actuators have typically been employed to mitigate the effects of low-to-medium magnitude earthquakes, turning to hydraulic actuators when in need to protect structures from strong earthquakes.

ISAAC
Paper publication – Structural team
An active mass damper for seismic protection of structures

However, low-maintenance and cost hydraulic actuators capable of improved performance are now achievable, thanks to recent breakthroughs and technological developments in the field. Examples include closed-loop systems whereby high-performance electric motors are used to generate the required oil flow and pressure, with lower space demands.

In this context, a novel servo-hydraulic AMD was proposed and developed that can be designed to enhance the target seismic performance of a building at multiple earthquake intensity levels [41]. Details pertaining to the electro-mechanical and electro-hydraulic components of this novel AMD, which represents the main object of this study, are provided in the following section.

The reliability and effectiveness of the newly proposed AMD were investigated via full-scale shake table test. Two nominally identical, reinforced concrete 3-story frame buildings were tested in the Eucentre laboratory in Pavia (Italy), subject to ground shaking of varying intensity. Both building specimens were intentionally designed to exhibit a "soft story" mechanism at the first level when subject to ground shaking of sufficient magnitude, but one was equipped with the proposed AMD, installed on the roof.

In the sections that follow, the results of the shake table experiments are discussed and used to draw some preliminary conclusions pertaining to the seismic performance of structurally deficient buildings retrofitted with the novel AMD, and to the effectiveness and general behavior of the AMD under realistic working conditions.

2 The proposed novel active mass damper

The AMD prototype tested in this work is shown in Figure 2. It is an innovative inertial system used as Active Vibration Control device that, differently from other AMDs, uses an electro-hydraulic actuator to move the inertial mass. The design, fabrication and preliminary testing of the prototype AMD has been carried out at the Politecnico di Milano, Italy. A brief description of the system is provided herein, while more details can be found in the companion paper by [41].

The AMD prototype is made up of a fixed part which transmits the force to the floor of the building it is connected to, and a moving part which is responsible for generating the control force. The latter has a weight of 2200 kg, while the overall weight of the system is 4000 kg. The plan dimensions of the device are 4.8 m by 1.5 m, the height is 1.3 m.
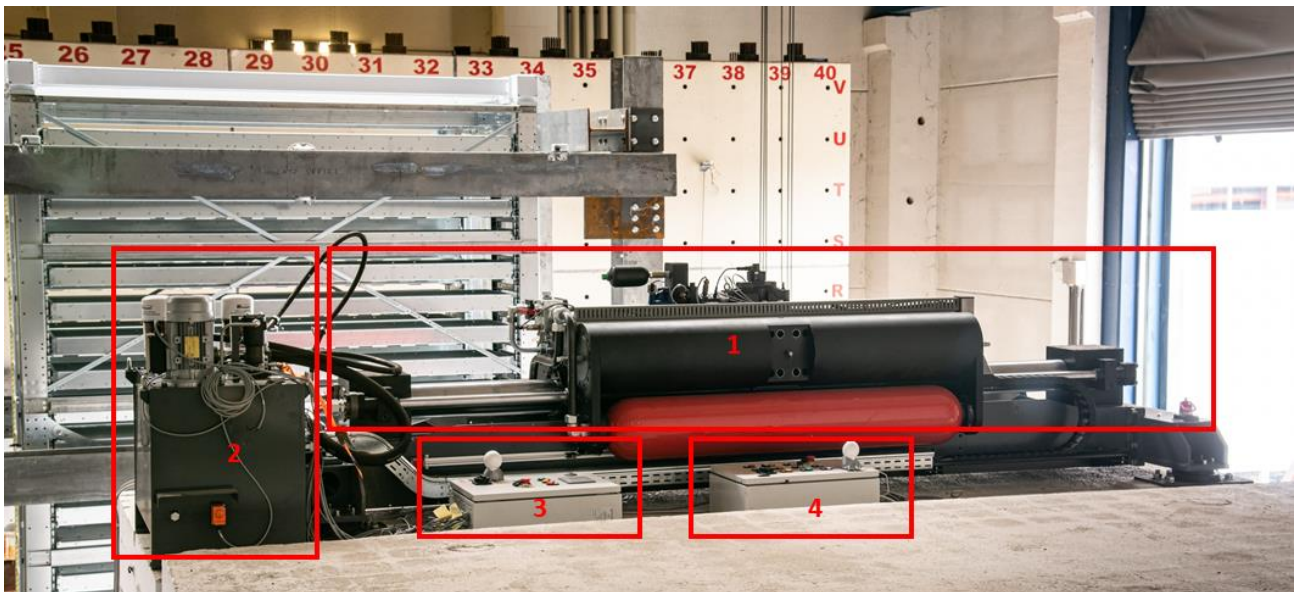

Figure 2 – The AMD proposed: 1) hydraulic cylinder; 2) oil restoration control unit; 3) control panel and fault management; 4) control panel and fault management of hydraulic control unit

The purpose of the AMD is to generate inertial forces that "counteract" the movement of the building by reducing the amplitude of oscillation and, consequently, the earthquake-induced forces experienced by the structural elements. The magnitude of the inertial forces to be generated is calculated in real time by the control algorithm, based on the accelerometric readings of sensors installed at certain locations across the structure.

Ideally, the AMD is to be installed on the roof of a building, with one or more devices acting in at least two orthogonal directions to reach the desired three-dimensional performance (optimal arrangement is determined on a case-by-case basis). It is also possible to install the AMDs at lower levels, if compatible with architectural and construction constraints. The AMD comprises four main subsystems: sensors, controller, actuators and power system.

The sensors are elements which provide the feedback needed for the control. They are installed on the structure to measure system response variables, such as displacements, velocities and accelerations. The sensors can also be used to perform tasks such as structural health monitoring, by allowing the dynamic identification of the structure during its life cycle.

The controller is the core of the AMD because it implements the vibrating control algorithm. It produces actuation signals by a feedback function of sensor measurements and defines the inertial mass displacement in time. Many types of control

ISAAC
Paper publication – Structural team
An active mass damper for seismic protection of structures

exist in the literature. The "Sky-Hook", a direct velocity feedback control which does not need the creation of a building model, was chosen for its performance and robustness. The algorithm defines a control force proportional to the relative velocity of the building and this force is produced by the double acting hydraulic actuator used to move the inertial mass. The actuator can generate a linear force up to 220 kN, with maximum velocity and displacement amplitude of 5 m/s and ±0.5m, respectively.

The AMD is connected to an Uninterruptible Power Supply (UPS) able to power all the electronic systems (controller, volumetric pump, electro-valve, etc.) in case of a blackout. The battery installed into the UPS can generate up to 3kW and provides power to the AMD, in absence of external current, for at least 24 hours. For context, in Italy the mean power recovery time for civil buildings is 8 hours.

The prototype has been tested and tuned via Hardware-In-the-Loop (HIL) simulations. In these hybrid analyses the AMD prototype was coupled with numerical models of case study buildings, to assess its behavior in real-time. These tests were used to study the response of the AMD and its effects on the structure at different earthquake intensities. Due to the limitations of the HIL test rig, earthquake inputs with a maximum PGA of 0.15g were simulated. Promising results were obtained, including reductions in roof displacements and accelerations of about 70% and 50%, respectively. During all tests, the AMD displayed excellent behavior, tracking with high accuracy the reference force to be generated.

3 Objectives and Scope

The current study aimed to investigate the proposed AMD under more realistic working conditions, further assessing its capabilities at enhancing the seismic performance of buildings. This was achieved via shake table testing of two nominally identical full-scale reinforced concrete frame structures with masonry infills, one of which equipped with the AMD, installed on the roof. The two specimens (described in more detail in Section 4.1) were not designed according to any particular design code and were not intended to be representative of any specific building typology or class of buildings. However, they were intentionally designed to exhibit a "soft story" mechanism at the first level when subject to ground shaking of sufficient magnitude. Soft story issues have been observed repeatedly and extensively over the course of past seismic events (e.g., Olive View Hospital during 1971 San Fernando, California earthquake [30]), making the case-study building ideal candidates to demonstrate the effectiveness of the proposed AMD at enhancing the seismic performance of realistic structures affected by a major structural deficiency.

In the sections that follow, the results of the shake table experiments are discussed and used to draw some preliminary conclusions pertaining to the behavior, reliability, and effectiveness of the proposed AMD, and to assess the enhanced seismic performance of AMD-retrofitted RC buildings.

4 Experimental Program and Setup

4.1 Description of the specimens

The elevation views of the nominally identical full-scale specimens are shown in Figure 3a). The two specimens were 3-story one-bay (in both directions) frame buildings, made of RC columns with 20 x 20 cm cross section, connected to 40 cm thick RC slabs. The columns were reinforced with 4 longitudinal 16 mm diameter steel bars in the corners, and 8 mm diameter closed stirrups spaced at 100 mm (Figure 3b).

The floor plan dimensions were 5.0 x 2.1 m, and the clear inter-story height was 2.5 m. Building A (not equipped the AMD) had a total height of 8.84 m, while Building B was 8.7 m tall. The different building height was due to the increased slab thickness (from 40 cm to 54 cm) at the roof level of Building A (see Figure 4). This was done to compensate the roof weight added by the AMD in Building B which resulted in a total increase of mass of only the 1%. It should be noted that in case of real structures, the weight added by the AMD system(s) is not expected to exceed 1% of the total weight of the building.

Infill masonry walls made of 8 x 25 x 25 cm clay blocks were installed in the N-S direction (i.e., the excitation direction) at each floor. The infill walls were coated externally with a layer of plaster and presented a series of openings, as shown in Figure 3a.

The two specimens were connected to the same foundation slab, which was bolted down to the shake table using post-tensioned steel bars. The distance between the two buildings was about 20 cm. A view of the buildings and AMD control system in their pre-test configuration is shown in Figure 4.
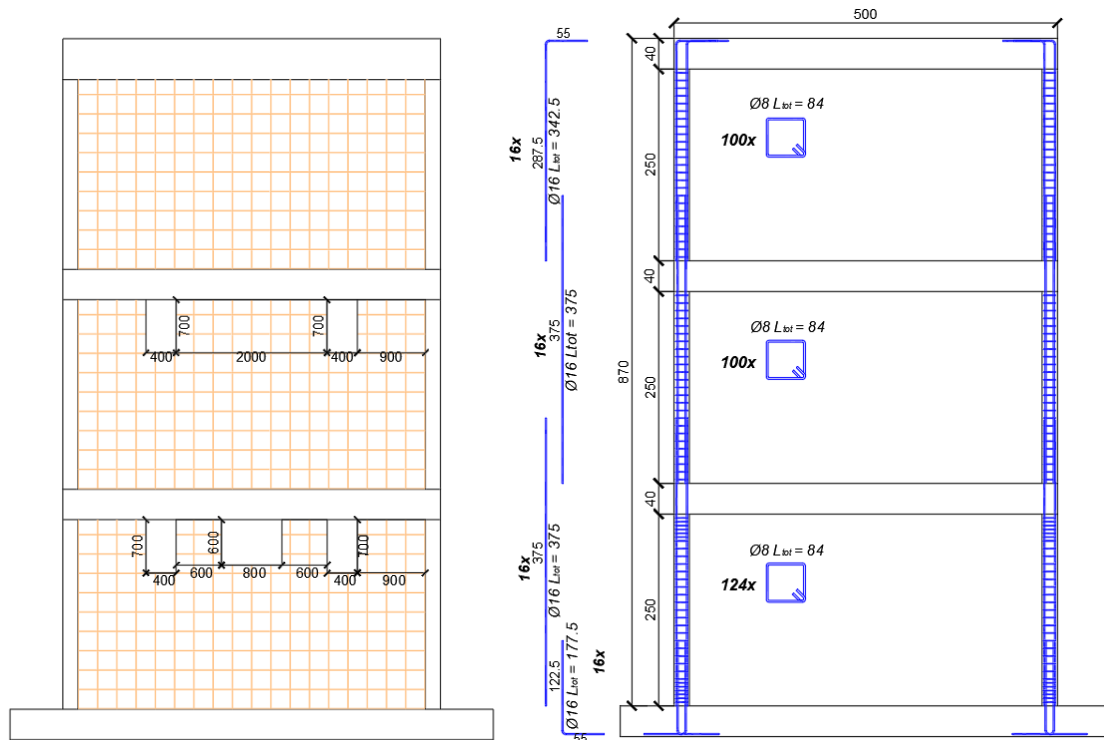
ISAAC
Paper publication – Structural team
An active mass damper for seismic protection of structures

Figure 3 - a) Elevation view of the buildings; b) Reinforcement details of the columns.
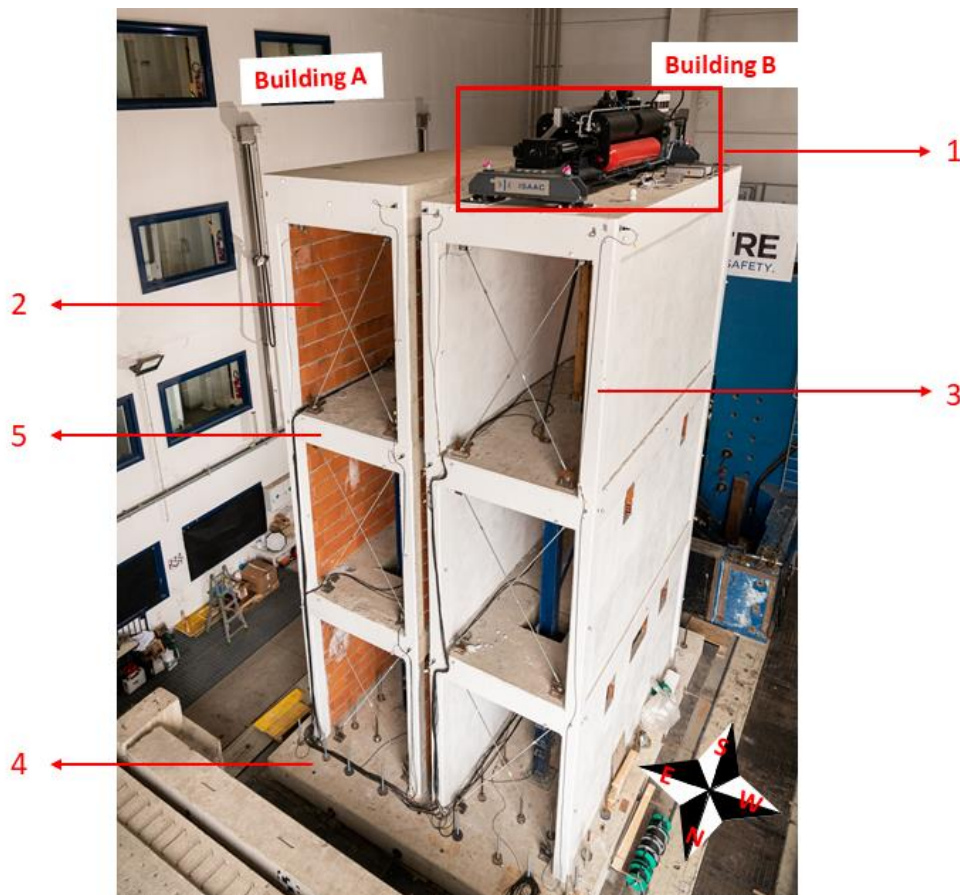

Figure 4 - The buildings tested in the Eucentre *laboratory: 1) AMD; 2) masonry infills; 3) columns; 4) foundation slab connected to the shake table; 5) floor slabs.*

ISAAC
Paper publication – Structural team
An active mass damper for seismic protection of structures

ISAAC

4.2 Setup of the AMD

The installation of the AMD system was performed considering three main aspects: the actuator position, the accelerometer locations and the control algorithm tuning.

Because the shake table tests conducted in this study were unidirectional, a single actuator was installed that could generate inertial forces in the direction of the ground shaking. The accelerometers for the structural dynamic's response feedback were placed on the specimens' foundation slab and at each floor, as described in section 4.4.

The control of the AMD is the "Sky-Hook" algorithm: a direct velocity feed-back control which does not need the creation of a building model. This vibration control can be seen as an equivalent damper element that connects the point of the structure where the control force is applied (the roof of the building) with the ground. The algorithm defines a control force proportional to the relative velocity of the roof of the building, computed as:

$$F_{control} = -Gain \cdot \dot{x}_{rel,roof} \qquad (1)$$

The Gain has to be properly tuned, in order to ensure performance and stability of the system in any working conditions. Furthermore, the AMD has a control logic algorithm which reduces dynamically the Gain coefficient during operation. This ensures the safety of the building in post-elastic regime when micro and macro cracks and other type of damage can occur, affecting the dynamic properties of the structure. These phenomena would impair the optimal functioning of the AMD (causing for example a reduction in performance and stability), if not properly compensated. For more details on the topic, see [41].

4.3 Experimental setup and loading protocol

The full-scale specimens described in the previous sections were tested on the unidirectional shake table in the Shake-LAB at the Eucentre facility, Italy. The table has dimensions 5.6 x 7.0 m and a maximum payload of about 1400 kN. The maximum acceleration of the empty table is 6g and the maximum displacement capacity is ±500 mm. The hydraulic system was designed and built to ensure high performance of the entire system. There are 8 pumps, able to provide a constant oil flow of 1360 lpm at a pressure of 280 bar, and 5 accumulation groups, which allow to further increase the flow rate for a short time if needed.

The specimens were tested by applying the E-W component of the Irpinia earthquake, which hit central Campania and central-northern Basilicata on the 23rd of November 1980. The main characteristics of this record are: a) peak ground acceleration PGA = 0.32 g; b) effective duration T_D = 6.32 s; c) Arias intensity Ia = 1.41 m/s; d) absolute cumulative velocity CAV = 10.88 m/s. The acceleration history record and acceleration response spectrum for the 100% intensity level are presented in Figure 5.
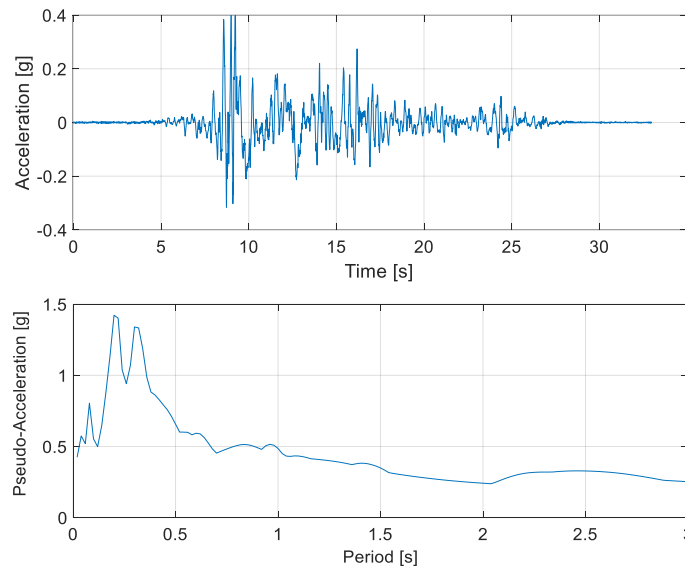

Figure 5 – a) Acceleration history of the reference record; b) pseudo-acceleration response spectrum at 5% damping

The shake table experiments were conducted in 5 phases, over the course of three days. Each testing phase involved the application of the Irpinia record (i.e., the reference earthquake), considering scale factors ranging from 0.10 to 1.37, as shown in Table 1. Column "CMP" reports the test IDs.

Table 1 – Loading protocol

ISAAC
Paper publication – Structural team
An active mass damper for seismic protection of structures

Day	Phase	CMP – ID test	Perc. of reference
1	1	1	10.0%
		2	17.5%
		3	25.0%
		4	32.5%
		5	40.0%
	2	6	45.0%
		7	50.0%
2	3	8	60.0%
		9	61.7%
		10	63.3%
		11	65.0%
		12	66.7%
		13	68.3%
		14	70.0%
3	4	15	10.0%
		16	30.0%
		17	50.0%
		18	70.0%
	5	19	137.0%

Furthermore, random wave tests were performed at the beginning of each testing phase. This technique was used to determine the progressive variation of the dynamic characteristics of the two buildings. These were then used to assess possible damage in the buildings that could not be detected visually.

Building damage assessment was also performed in real time, checking the output data at the end of each test. The measured displacements of the two buildings and the photographs of the damaged regions were compared. In addition, rapid visual inspections were performed, primarily to assess damage to the infill walls.

4.4 Instrumentation

The response of both the shake table and the specimens was monitored in real time through an array of instruments including 20 accelerometers (Figure 6a), 19 displacement transducers (Figure 6b) and an optical acquisition system (Figure 7).

The accelerometers were arranged as follows:
- One uniaxial accelerometer (oriented in the N-S direction) and one bi-axial accelerometer (monitoring both N-S and W-E-direction), were installed on the shake table and on the foundation slab, respectively. These were intended to measure the input acceleration at the base of the two buildings;
- 18 accelerometers were installed on the two buildings, three on each floor. Of these, two were installed in opposite corners and one was placed in the center of the floor slab. This arrangement was adopted to allow the monitoring of possible torsional behavior and/or rocking of the structures.

The displacement transducers were arranged as follows:
- 2 displacement transducers were used to monitor the relative displacement between the shake table and the foundation in both the horizontal and vertical direction;
- 1 displacement transducers was installed to record the displacement of the shake table relative to the bottom base plate;
- 12 wire displacement transducers were installed at the various floors, to record the floor displacements.

The optical acquisition system consisted of a series of infrared cameras used to continuously detect the position in space of a grid of reflective targets attached to the buildings, as outlined in Figure 7. In particular, the markers have been grouped on several levels. On the West side (Building B) 6 levels have been provided in correspondence of the floor slabs and of the columns centerline, for a total of 15 markers. On the North side, the markers have been applied with the same criteria on the two buildings, for a total of 12 markers on the Building A and 8 on the Building B.

ISAAC
Paper publication – Structural team
An active mass damper for seismic protection of structures

Figure 6 – a) View of installed accelerometer sensor; b) View of installed displacement transducers
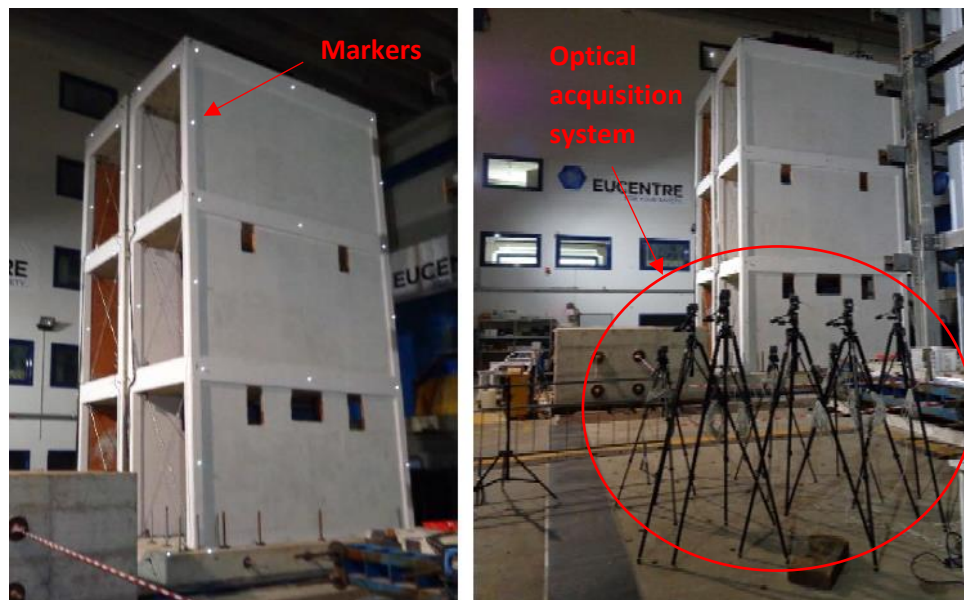

Figure 7 - Markers and optical acquisition system

5 Experimental Results

The results of the experimental program are summarized in this section. The results are mainly presented by reporting key aspects of the specimen behavior, with particular focus on the observed damage exhibited following each shaking level, and in terms of displacement time histories and peak displacements/drifts experienced by the two specimens.

5.1 Dynamic identification tests

Each testing phase was preceded by a structural dynamic characterization test. The purpose of these tests was twofold: on one hand, the dynamic properties and modal characteristics of the buildings were used to determine features such as lateral stiffness and to track its progressive degradation with damage; on the other hand, the outcome of the characterization tests was used to support the calibration of the finite element models of the specimens, implemented to perform numerical simulations of the shake table tests (not included in this paper).

The dynamic characterization was conducted by subjecting the structures to a sweep sine wave excitation generated by a 1.5 kg vibrodyn installed on the roof of the buildings. The buildings response was tracked via piezoelectric accelerometer sensors installed at the nodes of the buildings.

The key results of the Experimental Modal Analysis (EMA) are summarized in Table 2 and mode shapes 4th and 6th are outlined in Figure 8.

ISAAC
Paper publication – Structural team
An active mass damper for seismic protection of structures

The modes of vibration in the direction of interest (N-S direction) are the 4th and 6th, for both buildings. The values of the eigenfrequencies and the mode shapes are virtually identical, supporting the notion that the two specimens are dynamically equivalent.

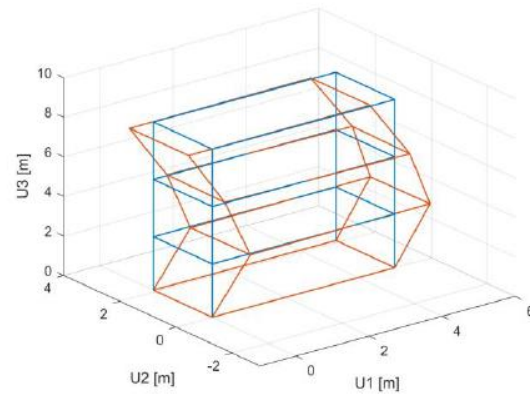*Table 2 – Results of experimental modal analysis*

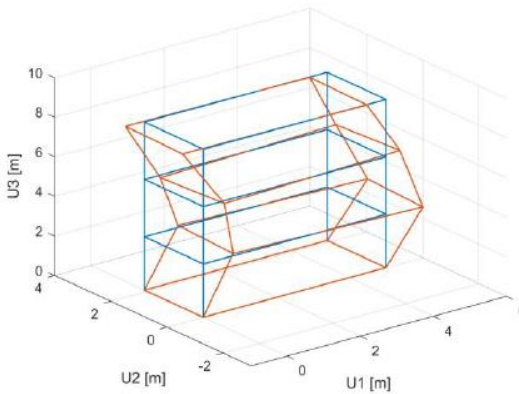| Specimen	Building A without active control		Building B with active control	
Mode	Frequency (Hz)	Direction	Frequency (Hz)	Direction
1	1.84	DY	1.93	DY
2	5.84	DY	6.13	DY
3	6.68	RZ	7.13	RZ
4	8.39	DX	8.38	DX
5	9.09	DY	9.25	DY
6	29.91	DX	31.91	DX
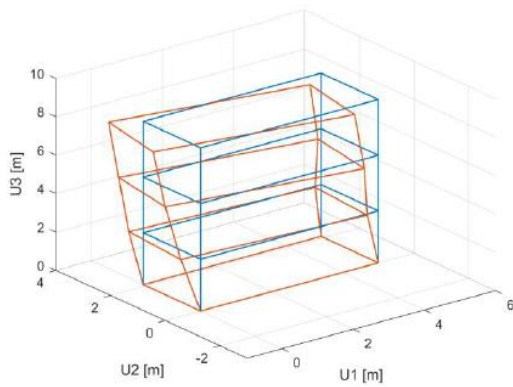
Building A Mode 4 - Frequency 8.38 Hz
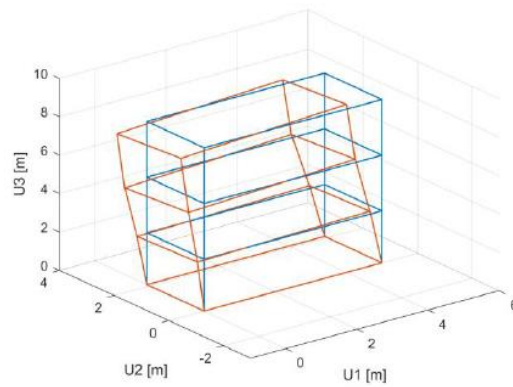
Building B Mode 4 - Frequency 8.39 Hz

Building A Mode 6 - Frequency 31.9 Hz

Building B Mode 6 - Frequency 29.9 Hz

Figure 8 - Experimental modal analysis

5.2 Damage progression

In this section, the performance of the specimens is assessed as a function of the level of damage detected following each test. The key observations are provided in Table 3 and can be summarized as follows:
- For earthquake intensities ranging from 10% to 60% of the reference input ground motion, both buildings exhibited essentially elastic behavior, with only a few small cracks (less 0.5 mm wide) occurring in the corner of infill panel at ground floor;
- For earthquake intensities ranging from 60% to 70% of the reference input ground motion, Building A (uncontrolled) suffered nontrivial widening of the existing cracks and experienced the formation of widespread

ISAAC
Paper publication – Structural team
An active mass damper for seismic protection of structures

new cracks in the infill walls of the ground floor; in contrast, Building B (controlled) only exhibited minor propagation of the pre-existing cracks;

- The 137% earthquake intensity (the largest scale factor considered) induced considerable damage in Building A that included extensive cracking and spalling of the infill walls in the top corner regions of the first floor (Figure 9a and Figure 10a) and structural damage in the form of diagonal cracks in the nodal panels of the slab-column connections. In contrast, Building B remained virtually undamaged (Figure 9b and Figure 10b), only exhibiting negligible widening of some of the cracks formed during previous testing phases.

Table 3 Summary of observed damage

Test ID	Scale Factor	Visible Damage	
		Building A	Building B
CMP 1 – CMP 5	10% - 40%	None	None
CMP 6 – CMP 7	40% - 50%	Small cracks	Small cracks
CMP 8 – CMP 18	60% - 70%	Enlarging cracks, new cracks	Enlarging cracks
CMP 19	137%	Partial collapse of infills, brittle collapse of slab-column panels at 1st floor.	Enlarging cracks at infills, no damage to RC elements

Figure 9 – Damage in the buildings after test CMP19: a) Building A visibly damaged, b) Building B virtually undamaged.

ISAAC
Paper publication – Structural team
An active mass damper for seismic protection of structures

a)	*b)*

Figure 10 – Detailed view of a selected region of the Buildings: a) cracking of the column-slab joint region of the first floor in Building A, b) column-joint region of Building B with no signs of distress.

The extensive damage experienced by Building A resulted into a reduction of lateral strength and lateral stiffness. Evidence of lateral stiffness reduction is provided in Figure 11, which shows the roof level accelerometer spectrogram of Building A. It is noting that the first natural frequency shifts from 8 Hz (undamaged building conditions) to 2 Hz (following test CMP19), that corresponds to the frequency of the bare frame, without the contribution of the infill walls. Building B, on the other hand, was characterized by an essentially elastic response exhibiting only minor damage to the infill walls and no damage to the reinforced concrete structural elements.
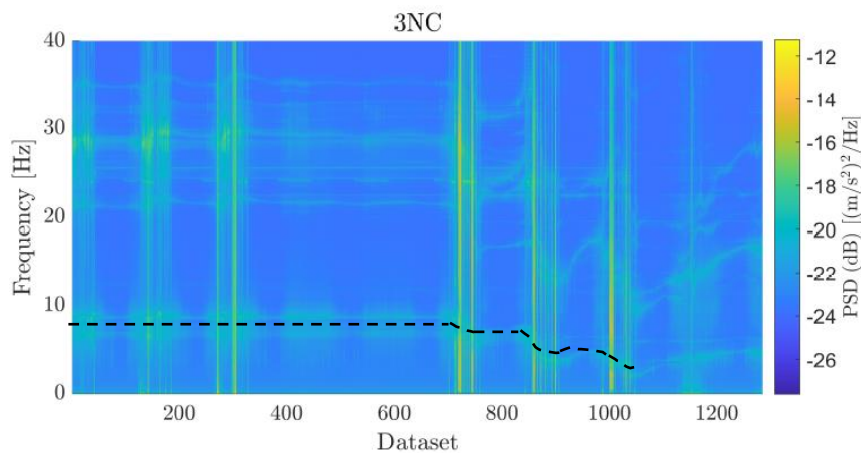

Figure 11 – Building A natural frequency trend.

5.3 Floor displacement time-history response

The floor displacement/drift results of the shake table tests are presented in this section. Figure 12 shows the peak first floor inter-story drifts for the two specimens during all testing phases. At shaking intensities ranging from 10% to 70% of the reference earthquake (CMP 1 to CMP 11), the maximum first story drift recorded for Building B was consistently 50% to 65% lower than that recorded for Building A. This is evidence that the AMD is beneficial and provides good control of the structural response at low-to-medium intensity shakings (i.e. at "serviceability" conditions).

The benefits of the AMD with respect to limiting the inter-story drift of the critical floor become even more prominent (and somewhat more relevant) in the case of high-intensity input ground motions. During test CMP 19, the first story of Building A reached a peak horizontal displacement of 22.5 mm, corresponding to a 0.90% inter-story drift ratio. For the same seismic input, the peak displacement of the first floor of Building B was only 6.3 mm, equaling an inter-story drift ratio as low as 0.25%. Thus, with the structures subject to high intensity shaking, the AMD induced a drift demand

ISAAC
Paper publication – Structural team
An active mass damper for seismic protection of structures

reduction of 72% at the critical level. As discussed in the previous section, this translates into a remarkable reduction of the extent of damage experienced by the building.
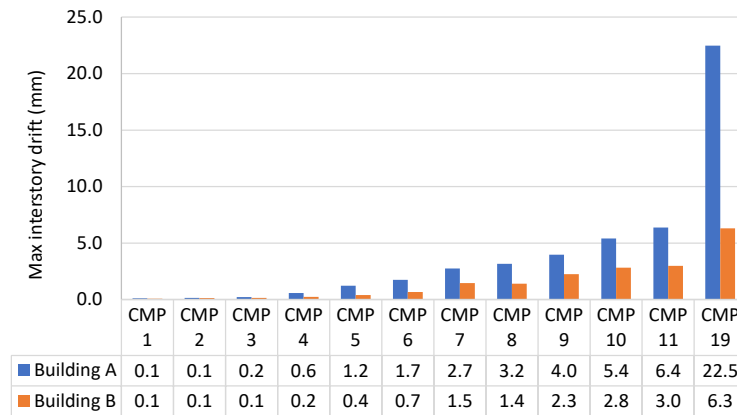

	CMP 1	CMP 2	CMP 3	CMP 4	CMP 5	CMP 6	CMP 7	CMP 8	CMP 9	CMP 10	CMP 11	CMP 19
Building A	0.1	0.1	0.2	0.6	1.2	1.7	2.7	3.2	4.0	5.4	6.4	22.5
Building B	0.1	0.1	0.1	0.2	0.4	0.7	1.5	1.4	2.3	2.8	3.0	6.3

Figure 12 – Graphical and numerical representation of the maximum interstory drift recorded at the first floor of both buildings during each test.

It is evident that the inter-story drifts for Building A were critical at the first floor (as per design objectives). However, while not explicitly shown here, they were relatively controlled at levels 2 and 3, with peak ratios recorded during test CMP 19 of 0.32% and 0.14%, respectively. At those same levels, Building B reached peak drift ratios of 0.18% (at both floors), thus exhibiting a uniform building response, with well-controlled drift values across the height. This is an excellent outcome as it confirms that the AMD successfully addressed the existing structural deficiency at the first floor, without compromising the structural response at other levels.

Figure 13 (left) shows the first floor inter-story drift for both Buildings A and B. All of Building A's peak drifts exceeding 20 mm are identified on the graph and marked with blue asterisks. The corresponding peak drift values recorded for Building B are marked with red circles. Note that there is a slight time misalignment between the peak displacements experienced by the two buildings (due to the different response of the two structures), but this offset never exceeds 0.5 s. It can be seen that the five largest peak drifts of Building B are, on average, about 18% of those recorded for Building A (3.94 mm against 21.42 mm). It is clear that this remarkable drift reduction is to be attributed to the contribution provided by the AMD. To emphasize this aspect, the AMD control force time history is provided in Figure 13 (right). The five force values corresponding to the peak displacements outlined in Figure 13 (left) are identified and marked. It can be seen that large forces with opposite sign with respect to the 1st floor inter-story drift detected for Building A are generated, that effectively counteract the movement of the building by reducing the amplitude of oscillation.
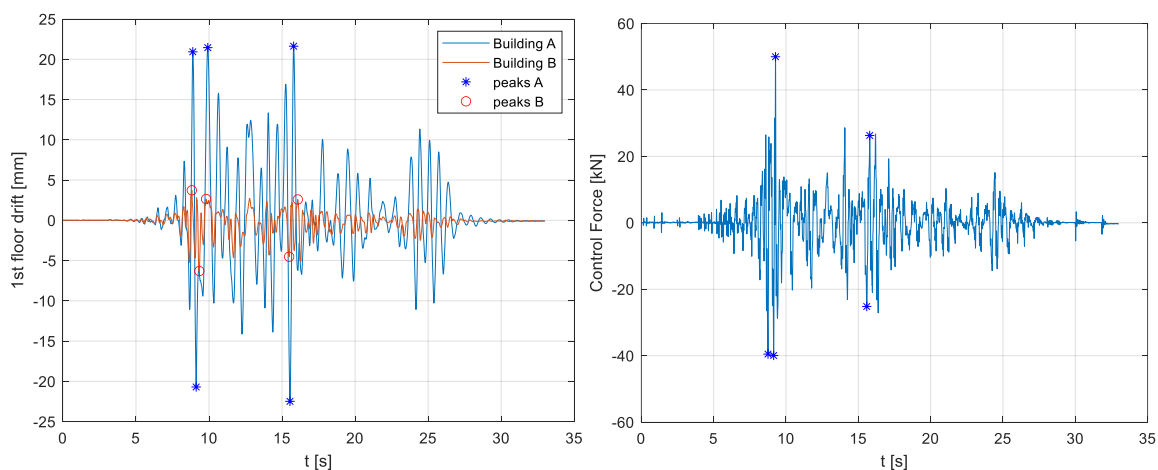

Figure 13 – First floor inter-story drift for both buildings (left) and AMD control force (right) during test (CMP 19)

ISAAC
Paper publication – Structural team
An active mass damper for seismic protection of structures

The peak data outlined in Figure 13 are summarized more clearly in Figure 14 and in Table 4. It is evident that the control force exerted by the AMD (yellow bar in Figure 14) opposes the 1st floor inter-story drift measured on the uncontrolled structure (blue bar), leading to a significant peak drift reduction for the controlled structure (orange bar).
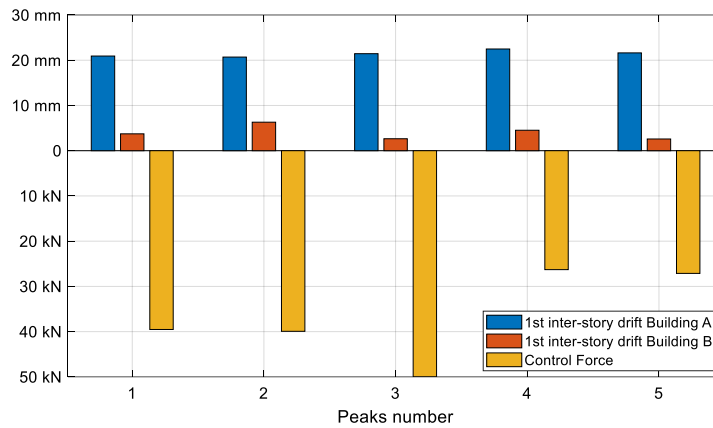

Figure 14 *- Five largest first floor inter-story drifts (Buildings A and B) and corresponding AMD forces (Building B) recorded during test CMP 19.*

Table 5 – Five largest first floor inter-story drifts and corresponding AMD forces recorded during test CMP 19.

Building A	*Time instant*	*8.9*	*9.1*	*9.9*	*15.5*	*15.8*
	Peak value	**20.9**	**20.7**	**21.4**	**22.5**	**21.6**
Building B	*Time instant*	*8.8*	*9.3*	*9.8*	*15.5*	*16*
	Peak value	**3.7**	**6.3**	**2.6**	**4.5**	**2.6**
AMD Control force (Building B)	*Time instant*	*8.8*	*9.1*	*9.3*	*15.8*	*16.4*
	Peak value	**39.5**	**39.9**	**50**	**26.3**	**27.1**

Figure *15* provides a snapshot of the deformed shapes of the two specimens at peak displacement, during test CMP 19. While this information is inherently included in the results presented above, the data displayed in Figure 14 provide more direct insight into the remarkably different response of the two buildings, emphasizing once again the beneficial contribution of the AMD with respect to the seismic performance of the structure. As discussed, Building B exhibits a very uniform response with inter-story drift ratios ranging from 0.25% to 0.18%. In contrast, the response of Building A is governed by a soft-story mechanism at the first floor, which reaches a peak inter-story drift ratio of 0.9%. For context, this value is 3 to 6 times greater than that recorded for the upper levels of Building A.
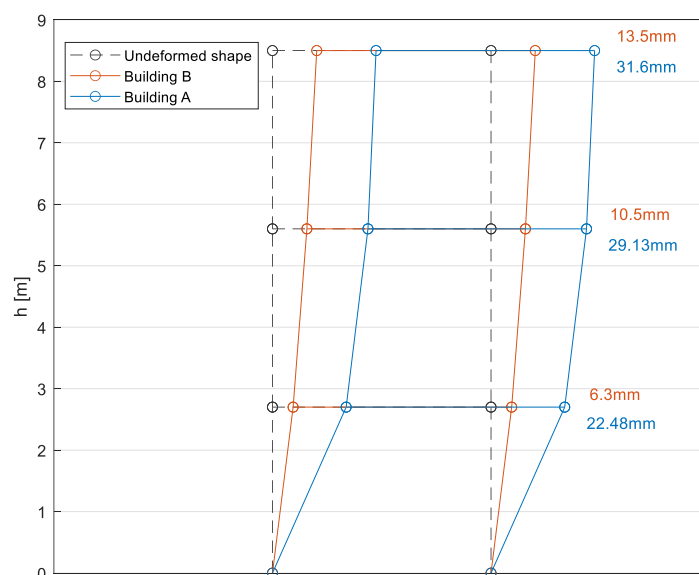

Figure 15 – Maximum displacement envelope for both buildings (CMP 19).

ISAAC
Paper publication – Structural team
An active mass damper for seismic protection of structures

6 Performance of the AMD

The experimental results discussed in the previous sections have demonstrated that the performance of the case study building was significantly enhanced by the presence of the AMD, in terms of inter-story drifts and overall damage to structural and non-structural elements.

This section focuses on the behavior of the AMD itself, to provide better insight into the role it plays with respect to the overall structural response. Only results pertaining to Test CMP 19 are presented, because it caused the most evident signs of distress in Building A, to both structural and non-structural elements.

The experimental results are presented primarily in terms of force-displacement response and energy dissipation characteristics of the AMD. This is because the inertial force generated and the amount of input energy absorbed by the AMD represent the two main aspects that contribute to enhancing the building seismic performance.

6.1 Behavior of the AMD

The AMD mass displacement and (generated) inertial force time-histories are shown in *Figure 16* and Figure 17. The Figures show that the maximum displacement of the mobile mass relative to the roof recorded during the strongest shaking was 116.7 mm, while the maximum inertial force generated by the AMD was approximately 51 kN. The AMD displacement and force limits are 500 mm and 220 kN, respectively. Thus, enhancing the performance of the case-study building tested in this study required the AMD to reach only 23% of its peak capacity.
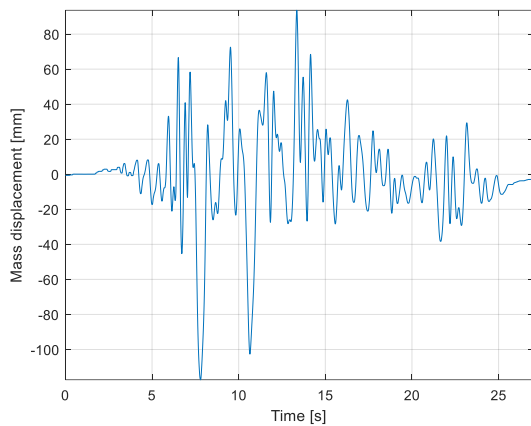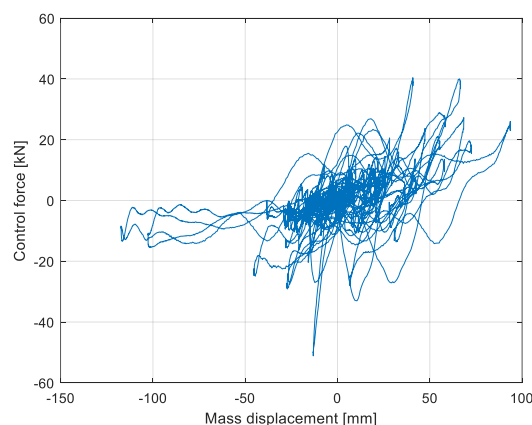

Figure 16 – AMD Mobile mass displacement during test CMP 19.
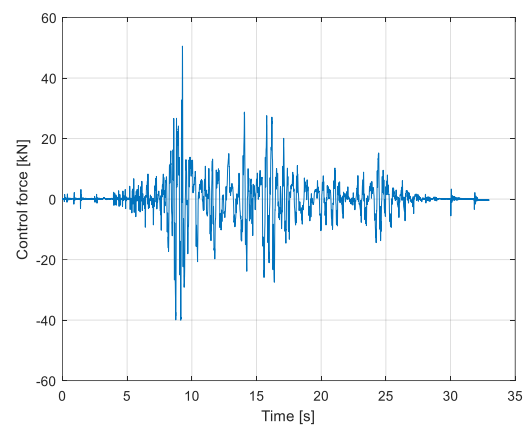
Figure 17 - Control force generated by the AMD during test CMP 19.

Figure 18 shows the relationship between the AMD inertial force and the displacement of the mobile mass. The diagram appears remarkably different from the typical response of passive devices, where the force-displacement cycles and hysteretic response are clearly visible. This is due to the active nature of the AMD control algorithms, which are based on feedback logic as explained in the previous chapters.

Thus, it is difficult to advance any considerations on the energy dissipation capabilities of the AMD, solely from the graph shown in Figure 18. However, an estimate of the energy absorbed by the system can be derived via energy balance approach. This is discussed in the next section of the paper.

Figure 18 - Relationship between control force and mobile mass displacements during test CMP 19.

ISAAC
Paper publication – Structural team
An active mass damper for seismic protection of structures

6.2 Energy dissipated

The energy dissipated by the AMD during shaking was computed idealizing the building as a 3-degree-of-freedom (DOF) shear-type structure with masses lumped at the floors, as shown in Figure 19 (an extra degree of freedom was considered to model the AMD in Building B). The floor masses m_1, m_2 and m_3 (treated as 1 DOF point masses) were estimated accounting for the floor slabs and the tributary mass of the adjacent columns; these are indicated using different colored areas in the 3D representation of the structure outlined in Figure 19. The floor columns were modeled as spring elements. Viscous damper elements were also included in the model at each level of the building.

The adopted modeling approach allows for both linear and nonlinear force fields to be adopted (the classic linear formulation is shown in brackets in grey color, Figure 19).
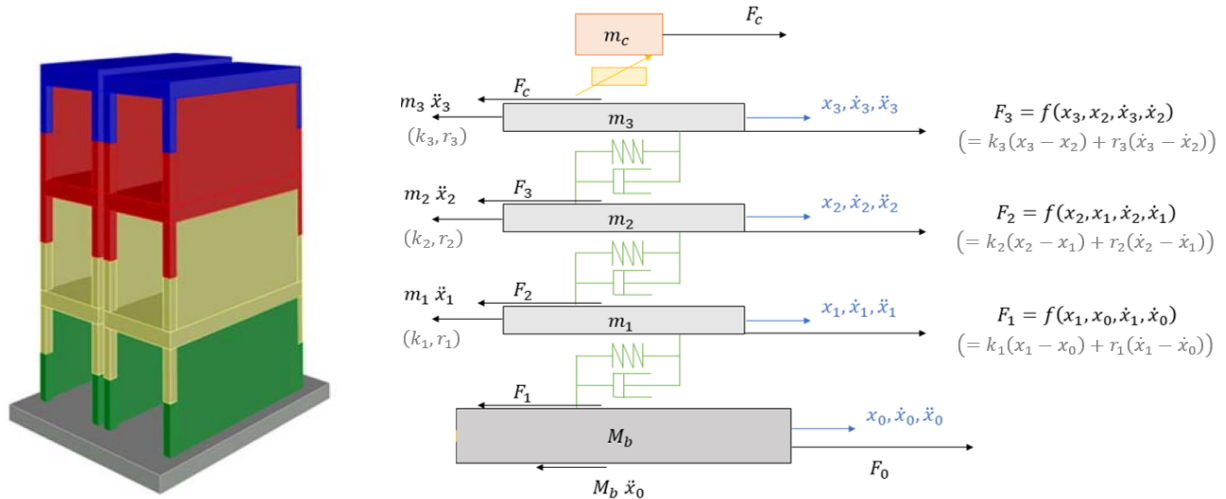

Figure 19 - Lumped-element model of the building

With reference to the model in Figure 19, the following dynamic equilibrium equations can be identified:

Equilibrium of the foundation slab	$F_0 = M_b \ddot{x}_0 + F_1$	(2)
Equilibrium of the 1st floor	$F_1 = m_1 \ddot{x}_1 + F_2 = m_1 \ddot{x}_1 + m_2 \ddot{x}_2 + m_3 \ddot{x}_3 + m_c \ddot{x}_c$	(3)
Equilibrium of the 2nd floor	$F_2 = m_2 \ddot{x}_2 + F_3 = m_2 \ddot{x}_2 + m_3 \ddot{x}_3 + m_c \ddot{x}_c$	(4)
Equilibrium of the 3rd floor	$F_3 = m_3 \ddot{x}_3 + F_c = m_3 \ddot{x}_3 + m_c \ddot{x}_c$	(5)
Balance on the AMD	$F_c = m_c \ddot{x}_c$	(6)

where:

- $\ddot{x}_0, \ddot{x}_1, \ddot{x}_2, \ddot{x}_3, \ddot{x}_c$ are the acceleration of each mass
- F_0 is the force that the facility actuators exert on the shake table
- F_1, F_2, F_3 are the restoring forces of the columns and infill walls of each floor
- F_c is the inertial force generated by the AMD (measured experimentally and set equal to 0 to model Building A)
- M_b is the mass of the foundation slab
- m_1, m_2 and m_3 are the masses associated to each floor
- m_c is the mobile mass of the AMD (set equal to 0 to model Building A)

The acceleration of each floor was measured experimentally, while the floor velocities were obtained by means of numerical integration of the acceleration signal, using an appropriate high-pass filter to avoid numerical drifts. These were used with Equations (2)-(6) to obtain the power balance equation outlined below (Eq. (7)). The energy absorbed by each floor and by the AMD was obtained by integrating the power terms. The sum of the energy absorbed by each floor, the energy dissipated by the AMD and the kinetic energy provides the total input energy of the earthquake. Because each energy term can be calculated from experimental data independently from the other energy terms, the overall balance can give a residual error. This was always checked to be negligible at steady state, to verify global equilibrium.

$$W_{in} = W_1 + W_2 + W_3 + W_c + \frac{dE_c}{dt} + err \qquad (7)$$

where:

1. $W_{in} = F_0 \dot{x}_0$ is the total power introduced in the system by the seismic force

ISAAC
Paper publication – Structural team
An active mass damper for seismic protection of structures

2. $W_1 = -(F_1 \dot{x}_1 - F_1 \dot{x}_0)$ is the power dissipated by the elements of the 1st floor
3. $W_2 = -(F_2 \dot{x}_2 - F_2 \dot{x}_1)$ is the power dissipated by the elements of the 2nd floor
4. $W_3 = -(F_3 \dot{x}_3 - F_3 \dot{x}_2)$ is the power dissipated by the elements of the 3rd floor
5. $W_c = -(F_c \dot{x}_c - F_c \dot{x}_3)$ is the power dissipated by the AMD at the roof
6. $\frac{dE_c}{dt} = M_b \ddot{x}_0 \dot{x}_0 + m_1 \ddot{x}_1 \dot{x}_1 + m_2 \ddot{x}_2 \dot{x}_2 + m_3 \ddot{x}_3 \dot{x}_3 + m_c \ddot{x}_c \dot{x}_c$ is the variation of kinetic energy of the system

The energy absorbed (comprehensive of the kinetic energy) by the various components of the structures is shown in Figure 20. Comparisons between total input energy and energy absorbed the structures and by the AMD are also provided in Table 6. Several observations can be made from the available data. For instance, the input energy for Building B is about 32% higher than for Building A (16.2 kJ and 12.6 kJ, respectively). However, the AMD dissipated roughly 63% of the total input energy, with the structure absorbing the remaining 37%. This corresponds to only 6.1 kJ, against the 12.6 kJ energy absorbed the structure of Building A. Thus, the energy dissipated solely by the structure in the AMD-equipped system was only 50% of the energy absorbed by the un-retrofitted building. Evidently, the lower the amount of energy to be absorbed, the lower the extent of damage to structural and non-structural elements. It is also interesting to notice that in the un-retrofitted case (Building A), about 71% of the total input energy was absorbed by the first floor. This is consistent with the results presented in the previous sections, and with the notion that the most severe seismic demand occurs at the first story that exhibited the greatest extent of damage and experienced the highest horizontal displacements. However, a much different trend is seen for Building B. By virtue of the AMD, there is a clear and favorable energy absorption shift whereby the amount of energy affecting the first floor is reduced to only 15% of the total input energy. This value is much closer to that observed for the second and third floors, indicating a much more uniform structural response. The reduction obtained on energy absorption of the overall structure is slightly more than 50%, but this percentage raises up to a 71% reduction on the first floor elements that are the most critical elements during a seismic event.
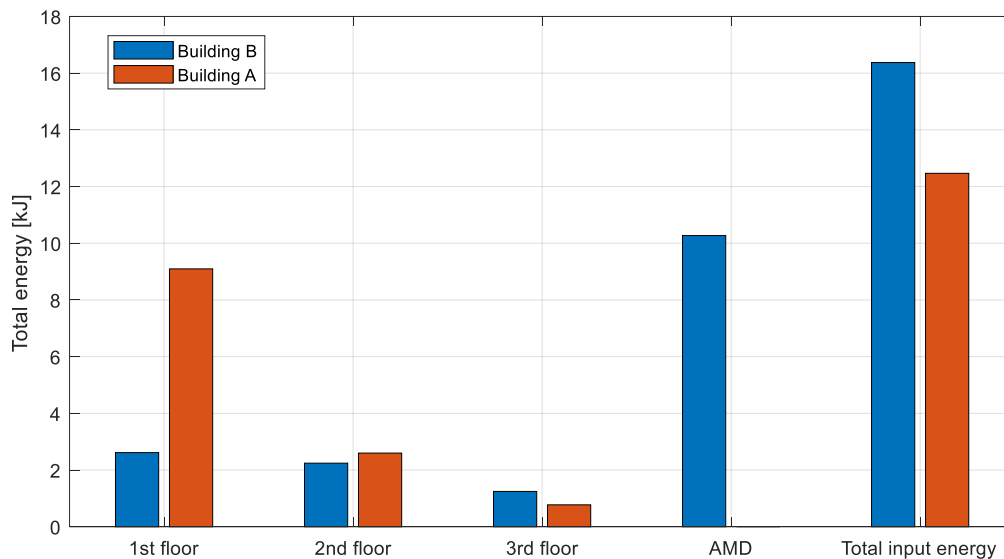

Figure 20 – Energy balance in both buildings (test CMP 19).

Table 6 – Energy balance in both buildings (test CMP 19).

	Building A	Building B
Energy absorbed by the structure [kJ]	12.6	6.1
Energy absorbed by the AMD [kJ]	-	10.2
Input energy [kJ]	12.6	16.3

7 Conclusion

Full-scale shake table tests were conducted to investigate the effectiveness of a newly proposed AMD, at protecting structurally deficient RC buildings from the effects of earthquakes. The operating principles of the tested AMD are based on the feedback received by sensors installed at strategic locations across the building. These measurements are processed by a central computer and the data elaborated via a control algorithm allow the actuator to move the inertial mass on the building roof. A control force is generated in real time that counterbalances the forces of inertia induced by the earthquake.

ISAAC
Paper publication – Structural team
An active mass damper for seismic protection of structures

The AMD was installed on the roof of one of two nominally identical full-scale RC frame building specimens, intentionally designed to exhibit a "soft story" mechanism at the first level. The buildings were tested on the unidirectional shake table available in the Shake-LAB at the Eucentre facility (Italy), under a real ground motion of increasing intensity. The experimental results showed that the un-retrofitted building (i.e., the building not equipped with the AMD) suffered significant structural and non-structural damage, particularly at the first floor of the building. In contrast, the AMD-retrofitted structure remained virtually undamaged even after being subject to the strongest shaking considered. It was shown that the AMD absorbed about two thirds of the total input energy, and provided excellent building protection, substantially reducing floor displacements and leading to a significantly more uniform building response. Most notably, the AMD induced a 72% reduction of the peak inter-story drift recorded at the critical level, effectively addressing the main structural deficiency that affected the case-study buildings. This reduction of the peak inter-story drift is consistent with the results of the energy balance that highlight a 71% reduction of energy absorbed by the elements of the first floor in the AMD-retrofitted building.

8 Aknowledgment

9 References

[1] FEMA P-366/April 2017. Hazus. Estimated annualized earthquake losses for the United States.

[2] Michael C. Constantinou, Tsu T. Soong, Gary F. Dargush, Passive Energy Dissipation Systems for Structural Design and Retrofit, Multidisciplinary Center for Earthquake Engineering Research

[3] S.J.Patil, G.R.Reddy, State Of Art Review - Base Isolation Systems For Structures - International Journal of Emerging Technology and Advanced Engineering, Volume 2, Issue 7, July 2012.

[4] Paolo M. Calvi, Gian Michele Calvi, Historical development of friction-based seismic isolation systems, Soil Dynamics and Earthquake Engineering 106 (2018) 14–30

[5] Ian Aiken, Passive Energy Dissipation – Hardware and Applications, Symposium on Passive Energy Dissipation Systems for New and Existing Buildings, Los Angeles July 1996

[6] M. C. Constantinou and M. D. Symans, Seismic Response Of Structures With Supplemental Damping, The Structural Design Of Tall Buildings, Vol. 2, 77 - 92 (1993)

[7] Mariantonieta Gutierrez Soto, Hojjat Adeli, Tuned Mass Dampers, Arch Comput Methods Eng (2013) 20:419–431 DOI 10.1007/s11831-013-9091-7

[8] Lyan-Ywan Lu, T.-K. L.-J.-H. (2018). Theoretical and experimental investigation of position-controlled semi-active friction damper for seismic structures. Journal of Sound and Vibration, 412, 184-206.

[9] Abe, M. (1996). Semi-active tuned mass damper for seismic protection of civil structures. Earthquake engineering and structural dynamics, 25(7), 743-749.

[10] F Weber, C. B. (2010). An adaptive tuned mass damper based on the emulation of positive and negative stiffness with an mr damper. Smart materials and structures, 20(1).

[11] Michael D. Symans a,*, Michael C. Constantinou, Semi-active control systems for seismic protection of structures: a state-of-the-art review, Engineering Structures 21 (1999) 469–487.

[12] F. Weber, Semi-active vibration absorber based on real-time controlled MR damper, Mechanical Systems and Signal Processing 46 (2014) 272–288.

[13] Felix Weber, Johann Distl, and Marcin Ma´slanka, Semi-Active TMD Concept for Volgograd Bridge

[14] Masato Abe, Semi-Active Tuned Mass Dampers For Seismic Protection Of Civil Structures, Earthquake Engineering And Structural Dynamics, Vol. 25,743-749 (1996)

[15] Marcin Ma´slanka and FelixWeber, Precise Stiffness Control with MR Dampers

[16] Xuan Bao Nguyen, Toshihiko Komatsuzaki, Yoshio Iwata, Haruhiko Asanuma, Modeling and semi-active fuzzy control of magnetorheological elastomer-based isolator for seismic response reduction, Mechanical Systems and Signal Processing 101 (2018) 449–466

[17] F Weber and M Ma´slanka, Frequency and damping adaptation of a TMD with controlled MR damper, Smart Mater. Struct. 21 (2012) 055011 (17pp)

[18] F Weber, Dynamic characteristics of controlled MR-STMDs of Wolgograd Bridge, Smart Mater. Struct. 22 (2013) 095008 (16pp)

[19] F Weber, C Boston and M Ma´slanka, An adaptive tuned mass damper based on the emulation of positive and negative stiffness with an MR damper, Smart Mater. Struct. 20 (2011) 015012 (11pp)

[20] Felix Weber, Hans Distl and Christian Braun, Semi-active Base Isolation of Civil Engineering Structures Based on Optimal Viscous Damping and Zero Dynamic Stiffness

ISAAC
Paper publication – Structural team
An active mass damper for seismic protection of structures

[21] Felix Weber, Hans Distl, Sebastian Fischer and Christian Braun, MR Damper Controlled Vibration Absorber for Enhanced Mitigation of Harmonic Vibrations, Actuators December 2016

[22] Ripamonti, F., Orsini, L., Resta, F. A Nonlinear Sliding Surface in Sliding Mode Control to Reduce Vibrations of a Three-Link Flexible Manipulator (2017) Journal of Vibration and Acoustics, Transactions of the ASME, 139 (5), art. no. 051005.

[23] Serra, M., Resta, F., Ripamonti, F. Dependent modal space control: Experimental test rig (2017) JVC/Journal of Vibration and Control, 23 (15), pp. 2418-2429.

[24] Ripamonti, F., Leo, E., Resta, F. Experimental and numerical comparison between two nonlinear control logics (2016) International Journal of Applied Mechanics, 8 (5), art. no. 1650061.

[25] Cinquemani, S., Diana, G., Fossati, L., Ripamonti, F. A smart structure for wind tunnel investigation of a bridge deck's vortex-induced torsional motion (2016) Mechatronics, 33, pp. 108-120.

[26] Cinitha, P. U. (2014). Enhancing the seismic response of buildings with energy dissipation methods-an overview. Journal of Civil Engineering Research, 4(2A), 17-22.

[27] Tarek Edrees Saared, G. N.-E. (2015). A state-of-the-art review of structural control systems. Journal of Vibration and Control, 21(9), 919-937.

[28] G De Roeck, G. D. (2011). A versatile active mass damper for structural vibration control.

[29] Elizabeth A Magliula, H. S. (s.d.). Vibration control of a two story buildig using active mass dampers. work.

[30] S.Dyke, B.Spencer, P.Quast, D.KaspariJr., M.Sain, Implementation of an active mass driver using acceleration feedback control ,Microcomput.Civil Eng. 11(1996)305–323.

[31] A.Forrai, S.Hashimoto, A.Isojima, H.Funato, K.Kamiyama, Gray box identification of flexible structures: application to robust active vibration suppression control, Earthq.Eng.Struct.Dyn.30(2001)1203–1220.

[32] C. Moutinho, A.Cunha, E.Caetano, Implementation of an active mass driver for increasing damping ratios of the laboratorial model of a building, J. Theor.Appl.Mech.49(2011)791–806.

[33] S. Chu, T.Soong, A.Reinhorn, Active Hybrid and Semi-Active Structural Control, John Wiley and Sons, Ltd, England,2005.

[34] T.Saito, K.Shiba, K.Tamura, Vibration control characteristics of a hybrid mass damper system installed in tall buildings, Earthq. Eng. Struct. Dyn. 30 (2001)1677–1696.

[35] H.B. Xu, C.W.Zhang, H.Li,J.P.Ou, Real-time hybrid simulation approach for performance validation of structural active control systems: a linear motor actuator based active mass driver case study, Struct. Control Health Monit. 21 (2014) 574–589.

[36] H.B. Xu,C.W.Zhang,H.Li,P.Tan,J.P.Ou,F.L.Zhou,Active mass driver control system for suppressing wind-induced vibration of the canton tower, Smart Struct.Syst.13(2014)281–303.

[37] M. Yamamoto, T.Sone, Behavior of active mass damper (AMD) installed in high-rise building during 2011 earthquake off pacific coast of Tohokuand verification of regenerating system of AMD based on monitoring, Struct.ControlHealthMonit.21(2014)634–647.

[38] J. Connor, S.Laflamme, Structural Motion Engineering, Springer International Publishing, Switzerland, 2014.

[39] M. Yamamoto, T.Sone, Behavior of active mass damper (AMD) installed in high-rise building during 2011 earthquake off pacific coast of Tohokuand verification of regenerating system of AMD based on monitoring, Struct.ControlHealthMonit.21(2014)634–647.

[40] Y.Nakamura, K.Tanaka, M.Nakayama, T.Fujita, Hybrid mass dampers using two types of electric servomotors: AC servomotors and linear-induction servomotors, Earthq. Eng. Struct. Dyn. 30(2001)1719–1743.

[41] M.Rosti, S.Cii, A.Bussini, F.Ripamonti, Design and Validation of a Hardware-In-the-Loop Test Bench for the Performance Evaluation of an Active Mass Damper, Journal of Vibration and Control, to be published.